HAL open science

Carbon content evolution in austenite during austenitization studied by in situ synchrotron X-ray diffraction of a hypoeutectoid steel

B. Denand, V.A. Esin, M. Dehmas, G. Geandier, S. Denis, T. Sourmail, E. Aeby-Gautier

To cite this version:

B. Denand, V.A. Esin, M. Dehmas, G. Geandier, S. Denis, et al.. Carbon content evolution in austenite during austenitization studied by in situ synchrotron X-ray diffraction of a hypoeutectoid steel. Materialia, 2020, 10, pp.100664. 10.1016/j.mtla.2020.100664 . hal-02985508

HAL Id: hal-02985508

https://hal.univ-lorraine.fr/hal-02985508v1

Submitted on 22 Aug 2022

HAL is a multi-disciplinary open access archive for the deposit and dissemination of scientific research documents, whether they are published or not. The documents may come from teaching and research institutions in France or abroad, or from public or private research centers.

L'archive ouverte pluridisciplinaire **HAL**, est destinée au dépôt et à la diffusion de documents scientifiques de niveau recherche, publiés ou non, émanant des établissements d'enseignement et de recherche français ou étrangers, des laboratoires publics ou privés.

Distributed under a Creative Commons Attribution - NonCommercial 4.0 International License

Version of Record: https://www.sciencedirect.com/science/article/pii/S2589152920300818
Manuscript_ac62f113ec527ae35fc4ee5a495cac10

Carbon content evolution in austenite during austenitization studied by in situ synchrotron X-ray diffraction of an hypoeutectoid steel

B. Denand[a,c], V.A. Esin[a,b], M. Dehmas[a,d], G. Geandier[a,c], S. Denis[a,c], T. Sourmail[e], E. Aeby-Gautier[a,c]

[a] Institut Jean Lamour, Université de Lorraine, CNRS, UMR7198, 54011 Nancy Cedex, France

[b] presently at MINES ParisTech, PSL University, Centre des Matériaux (CMAT), CNRS UMR 7633, BP 87, 91003 Evry, France

[c] Laboratory of Excellence for Design of Alloy Metals for Low-mass Structures ('DAMAS' Labex), Université de Lorraine, France

[d] presently at CIRIMAT, Université de Toulouse, CNRS, Toulouse, France

[e] Ascometal-CREAS (Research Centre), Hagondange, France

Abstract

Using in situ high energy X-ray diffraction study of austenite formation in hypoeutectoid steel with three different initial microstructures (ferrite-pearlite, tempered martensite and bainite), the lattice parameters of ferrite, cementite and austenite are examined on heating at 0.25, 10 and 100 °C/s.

The lattice parameters of ferrite, cementite and austenite do not vary linearly with the temperature, especially, in the temperature range where the austenitization takes place. For the austenite, it is suggested that the deviation from the linearity is mainly associated to the

© 2020 published by Elsevier. This manuscript is made available under the CC BY NC user license
https://creativecommons.org/licenses/by-nc/4.0/

carbon content variation. Using Dyson and Holmes equation, the carbon content in austenite is evaluated for any moment of the austenite formation for each initial microstructure and all heating rates.

For the ferrite-pearlite microstructure heated at 0.25 °C/s, the carbon content in austenite after complete cementite dissolution corresponds to that of pearlite. Moreover, a rapid decrease in carbon content in the austenite is observed during the first stage of the austenitization (simultaneous dissolution of ferrite and cementite) followed by a slow further decrease during the transformation of the remaining ferrite. The obtained results are discussed using thermodynamic calculations.

Keywords: Austenitization, In situ synchrotron X-ray diffraction, lattice parameter, carbon content, Thermo-Calc

1. Introduction

The service life of crankshafts for automotive industry can be increased by surface hardening via an induction heat treatment [1,2]. Such a local heat treatment leads to a formation of austenite close to the surface which further transforms into martensite upon subsequent quenching. Therefore, the resulting surface layer has a higher hardness in comparison with that of the bulk. In addition, retained compressive stresses are generated in the surface layer (mainly due to the martensitic transformation in that area), optimal for the properties of crankshafts use [3].

The required heat treatment should be fast enough to limit the volume of the material transformed into austenite (close to the surface) on heating. Typical heating rates vary from 30 to over 100 °C/s. In these conditions, the initial microstructure of the steel may affect

the austenitization kinetics due to differences in interface migration and interstitial and substitutional elements redistribution in different microstructures. Even for a fully austenitic layer, the chemical composition may present local heterogeneities due to initial microstructure features leading thus to local differences in final microstructure with different local mechanical properties. It is worth noting, that most of investigations reported in literature have been carried out on the austenitization of steels with initial ferrite-pearlite microstructure [4-14]. The analysis of austenite formation for the same steel having different initial microstructures and for different heating rates is of technological and fundamental importance. In this scope, our previous study reported on the kinetics of austenite formation considering three initial microstructures (ferrite-pearlite, tempered martensite and bainite) of the same hypoeutectoid steel and five heating rates (0.25, 1, 10, 60 and 100 °C/s) [15]. The use of High Energy synchrotron X-Ray Diffraction (HE-XRD) [16] allowed to characterize the phase fraction evolution of all phases and highlighted two steps in the austenite formation [15]: i) the simultaneous transformation of ferrite and cementite into austenite, and ii) the transformation of the remaining ferrite into austenite. For a given heating rate, the kinetics of each step was shown to be dependent on the initial microstructure.

In addition to the nature and amount of phases formed, the Rietveld refinement of diffraction patterns gives also information about the lattice parameters and widths of diffractions peaks for different phases for any moment during heating and the austenite formation. To get insight into the transformation features, the present paper focuses on the evolution of lattice parameters of austenite, ferrite and cementite to be able to estimate the carbon content evolutions in the phases.

It is worth noting that a recent study attempted to analyse the evolution of austenite lattice parameter during austenitization of the same 50CrMo4 steel having ferrite-pearlite and soft annealed initial microstructures close to equilibrium state [14]. In situ HE-XRD was used on heating with the rates of 1, 10 and 100 °C/s. A decrease in austenite lattice parameter was observed at the beginning of the austenite formation until a minimum value followed by further linear increase with temperature. Such a change in austenite lattice parameter was qualitatively attributed to the evolution of austenite chemical composition. However, any attempt was not done to quantify austenite carbon content or lattice parameter evolution of ferrite cementite and austenite, and only possible explanations were given.

In the present work an accurate analysis of X-ray data is carried out using Rietveld refinement. Different assumptions concerning the evolution of lattice parameters of ferrite, cementite and austenite are carefully analysed to be able to obtain the austenite carbon content at any moment of the transformation for different heating rates. Besides, non-equilibrium tempered martensite and bainite microstructures are investigated together with ferrite-pearlite initial microstructure.

2. Material

The steel used in the present work is a 37MnCr4-3, which provided by was manufactured by Ascometal CREAS. The chemical composition was characterized on forged bars using optical emission spectrometry and combustion (LECO) analysis for accurate measurements of carbon and sulphur contents (**Table 1**). The steel was made available as hot forged bars of approximate diameter 40 mm. Details of the fabrication process have already been reported in Ref. [15].

Table 1. Chemical composition (wt. %) of the 37MnCr4-3 steel used

Fe	C	Si	Mn	S	Ni	Cr	V	Mo	Cu	Al
Bal.	0.356	0.253	1.285	0.024	0.208	0.652	0.005	0.065	0.172	0.018

To produce different initial microstructures, the forged bars were austenitized at 850 °C for 1 hour and further subjected to different heat treatments. These thermal treatment have already been detailed in [15], but will nevertheless be summarised for ease of legibility. To obtain ferrite-pearlite initial microstructure, the steel was air cooled from austenitizing temperature down to 625 °C and held at this temperature for 1 hour. The tempered martensite required oil quenching at room temperature from austenite domain followed by a tempering at 500 °C during 1 hour. The bainite microstructure was obtained during an isothermal soaking in a salt bath at 450 °C during 30 minutes after austenitizing.

The samples used in this study were taken at the mid radius of the bars for each initial microstructure in order to avoid decarburization phenomenon at the surface of these bars. These initial microstructures obtained by Scanning Electron Microscopy (SEM) are presented Fig. 1.

Fig. 1a shows the initial ferrite-pearlite microstructure where black regions are the free ferrite and grey regions are the pearlite. Volume fraction of ferrite and pearlite can be determined by image analysis based on contrast threshold. The mean phase fraction obtained for the free ferrite is 20% and that for the pearlite is 80%. , The intercepts method allowed us to estimate the size of mean pro-eutectoid ferrite grains to be of 10 µm. For the initial tempered martensite and bainite microstructures (Fig. 1b-c), it was not possible to distinguish the different phases by SEM.

HE-XRD analysis revealed the presence of about 2-3 wt.% of cementite for the three initial microstructures and 3 wt.% retained austenite in the bainitic microstructure.

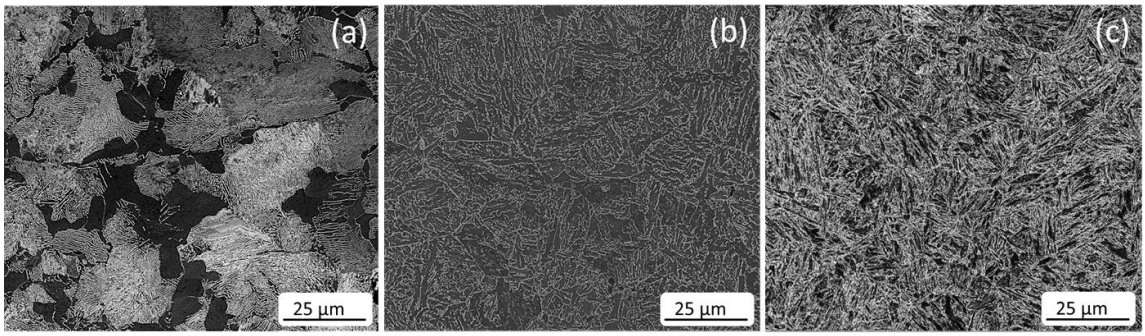

Fig. 1. Initial (a) ferrite-pearlite, (b) bainite and (c) tempered martensite microstructures of the investigated steel as observed by SEM (standard metallography preparation and 2% Nital etching).

3. Experimental techniques

Experiments were carried out at the Deutsches Elektronen-Synchrotron (DESY, Hamburg, Germany) on the beamline P07 of PETRAIII. A DIL805 A/D dilatometer from TA Instrument was used to apply the thermal treatments. Three linear heating rates (0.25, 10 and 100 °C/s) were imposed until 900°C followed by gas quenching.

The samples were hollow cylinders of 10 mm length whose the external diameter was 4 mm and the thickness was 0.5 mm in order to reduce radial thermal gradient.

Induction heating was employed during the experiments and the temperature was controlled using S-type thermocouple centrally welded at the surface of the hollow cylinder. In order to have a good correlation between the temperature acquisition and the Debye-Sherrer rings recorded during the thermal treatment, the X-ray beam crossed the sample in the area close to thermocouple. The Debye-Scherrer rings were obtained by using a monochromatic beam of 100 keV and 2D image plate detector situated at about 1.5 m away from the sample. A preliminary calibration with CeO_2 powder was carried out to determine the values required for further X-ray data analysis such as the distance between the sample and the detector or the wavelength which was 0.123984 Å in this case. The beam size of 1.0 × 1.0 mm² allowed getting a reasonably good resolution and fast acquisition time for the high heating rates. Indeed, two modes were employed to the diffraction pattern recording: a slow mode

with an acquisition time of 3.5 s for the heating rate of 0.25°C/s and a fast mode with an acquisition time of 0.1 s for the heating rates of 10 and 100 °C/s. For the slow mode, the acquisition time included the shutter opening and closing, the acquisition of external parameter as the temperature, and the data erasing from the detector. In the fast mode, the shutter opened at the beginning of the experiment and closed at the end; any external parameter was not recorded during the acquisition.

The fast mode led thus to an uncertainty in temperature value which can be calculated as $\Delta T = \pm 0.1 \times V_h$, where V_h (°C/s) is the heating rate and 0.1 (s) is the acquisition time in fast mode.

It is worth noting that for the present study three heating rates were selected: 0.25, 10 and 100 °C/s while 1 and 60 °C/s heating rates were used as well in the study on austenitization kinetics in the same steel in Ref. [15].

The Debye-Scherrer rings give information on the sample crystallography at any moment during the thermal path. The complete integration of these rings leading to conventional 1-D diffractograms were made using the Fit2D software. Then, the diffractograms were analysed by Rietveld refinement [17,18] with the FullProf software [19].

The starting structures for the Rietveld analysis consisted of ferrite and cementite for the initial ferrite-pearlite and tempered martensite microstructures, and of ferrite, cementite and austenite for the analysis of the bainitic microstructure. More details concerning the procedure of Retvield refinement can be found in the Ref. [15]

For each XRD pattern, the following parameters were refined: scale factors, mass fractions, FWHM (full width at half maximum) and lattice parameters.

4. Results

The kinetics of austenite formation as a function of initial microstructure and heating rate was reported in details in Ref. [15]. We recall here the main results and conclusions required for the further analysis of the lattice parameters evolutions.

The temperature range of austenite formation on heating for different conditions is given in **Table 2**. In order to obtain a good confidence on these temperatures, the start of austenitization (A_{C1}) is taken for a mass fraction of 3% of austenite created and the ferrite dissolution is considered as completed (A_{C3}) for 95% of austenite formation.

Table 2. The temperatures of the start (A_{C1}) and end (A_{C3}) of austenite formation on heating as well as the temperature of the end of the first stage of austenite formation (T_1) according to the data obtained from HE-XRD experiments in Ref. [15] for different initial microstructures and heating rates

	Ferrite-pearlite			Tempered martensite			Bainite		
Heating rate (°C/s)	A_{C1} (°C)	T_1 (°C)	A_{C3} (°C)	A_{C1} (°C)	T_1 (°C)	A_{C3} (°C)	A_{C1} (°C)	T_1 (°C)	A_{C3} (°C)
0.25	740	753	790	736	758	774	736	763	770
10	761	792	822	743	763	779	741	769	790
100	781	843	854	753	788	810	743	789	810

The data reported in **Table 2** clearly evidence that the transformation kinetics is depending on the initial microstructure, mainly the size of the different microstructure constituents [15]. The phase fraction evolutions show two stages in the kinetics of austenite formation. The first one corresponds to the simultaneous dissolution of ferrite and cementite; the second one to the dissolution of the remaining ferrite. The temperature of the end of the first stage (T_1) is recalled in **Table 2**. This temperature is dependent on the initial microstructure and heating rate and its variation was attributed to different size of cementite particles in different initial microstructures [15].

Together with phase fractions, the results of Rietveld refinement inform about evolution of the mean lattice parameters of ferrite, cementite and austenite. Those are further analysed

and discussed considering the different origins of lattice parameter evolution: the temperature variation, the elastic strains and/or the variation of chemical composition of different phases during austenitization.

4.1 Mean lattice parameters on heating

The variation of mean lattice parameters of ferrite and austenite during heating with a rate of 0.25 °C/s is given in **Fig. 2** for the three initial microstructures. For cementite, the change in unit cell volume on heating is reported in **Fig. 3** for the same conditions. The values of apparent coefficients of thermal expansion, obtained in the temperature ranges where no transformation occurred, are summarized in **Table 3** for all phases[1].

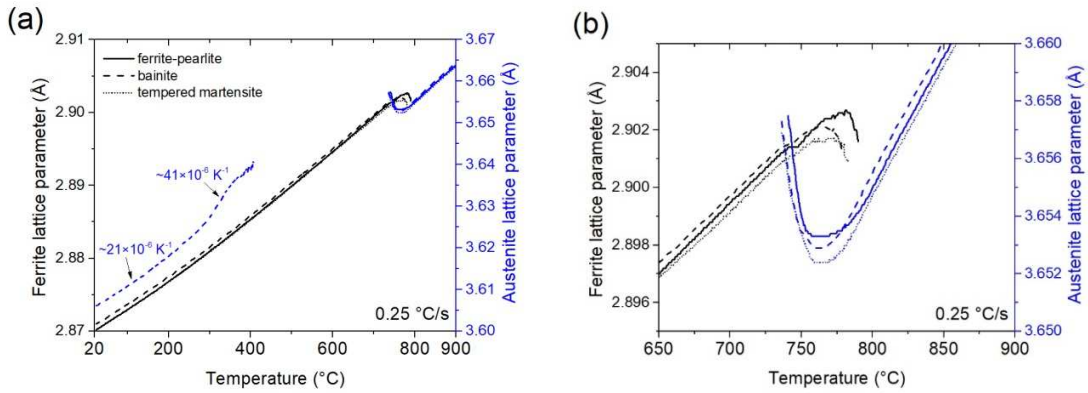

Fig. 2. Mean lattice parameters of ferrite and austenite on heating with a heating rate of 0.25 °C/s for initial microstructures of ferrite-perlite (solid), bainite (dashed) and tempered martensite (dotted): (a) before, during and after austenitization and (b) zoom to the temperature range where the austenite formation occurs.

[1] The volume thermal expansion coefficients of cementite were measured in the temperature range 450-600 °C for two reasons: i) theses temperatures are higher than cementite Curie temperature (T_c≈227 °C) [20] (magnetic transition has a significant effect on the thermal expansion coefficient in a temperature range of about 200°C around T_c); ii) for the initial bainite microstructure some transformation of the retained austenite occurred for temperatures lower than 450 °C and may affect the apparent thermal coefficient of cementite.

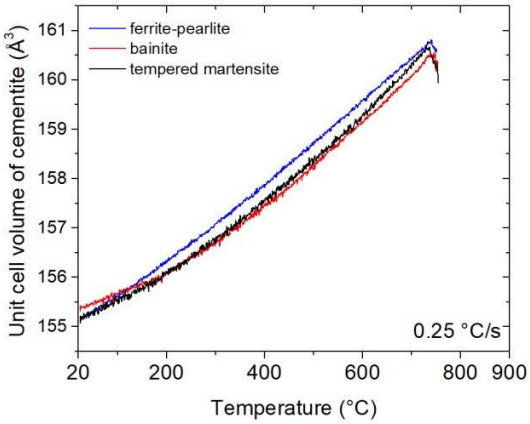

Fig. 3: Unit cell volume of cementite before and during austenitization with a heating rate of 0.25 °C/s for initial microstructures of ferrite-pearlite (blue), bainite (red) and tempered martensite (black)

Table 3. Volume coefficient of thermal expansion of cementite in the temperature range from 450 to 600 °C, and linear coefficient of thermal expansion of ferrite and austenite in the temperature range where no transformation occurs

Coefficient of thermal expansion (10^{-6} K^{-1})	Initial microstructure			Literature data
	Ferrite – pearlite	Bainite	Tempered martensite	
Volume, cementite	54	56	54	46 [25], 58 [26]
Linear, ferrite	16.4	16.2	16.1	14-16 [20,21], 16.3 [23], 16.8 pure iron [23], 16 [25]
Linear, austenite	24.7	24.9	24.4	20-23 [20], 24 [21]

For the ferrite-pearlite and tempered martensite initial microstructures that contain a mixture of ferrite and cementite, the mean lattice parameter of ferrite increases linearly with temperature up to 735 °C. Between 735 °C and around 760 °C, in the first stage of the austenite formation, the mean lattice parameter of ferrite slightly deviates from the linear behaviour, with a decrease in the apparent Coefficient of Thermal Expansion (CTE). Above 760 °C (**Fig. 2b**), in the second stage of the transformation, the lattice parameter of ferrite decreases with a negative apparent CTE. For both ferrite-pearlite and tempered martensite microstructures, the unit cell volume of cementite increases with increasing temperature: a linear behaviour is only observed between 450 and 735 °C (**Fig. 3**). Above 735 °C where

cementite dissolution occurs, a decrease in the unit cell volume of cementite is observed. For the bainite microstructure, the initial state contains a mixture of three phases (ferrite, cementite and retained austenite). During the heating between 240 and 410 °C, the transformation of retained austenite into ferrite and cementite occurs. Between 410 and 735 °C, the amount of ferrite and cementite remains constant. Nevertheless, the mean lattice parameters of ferrite and cementite have almost a similar evolution than the one obtained for ferrite-pearlite and tempered martensite microstructures.

For the evolution of austenite lattice parameter, two temperature ranges should be distinguished: (i) above 730 °C where a mixture of ferrite and cementite transforms into austenite (ferrite-pearlite, tempered martensite and bainite microstructures), and (ii) between 240 and 410 °C where retained austenite transforms into ferrite and cementite (bainite microstructure only).

A complex non-linear evolution of austenite lattice parameter with temperature is observed during the ferrite+cementite→austenite transformation whatever the initial microstructure (**Fig. 2b**). A significant decrease in austenite lattice parameter is observed between 735 and 760 °C, during the first stage of the transformation. Above 760 °C, during the second stage of the transformation, the austenite lattice parameter increases. The CTE of austenite increases until reaching a constant value of 25×10^{-6} K^{-1} once the transformation is completed.

For initial bainitic microstructure, the CTE of retained austenite obtained between room temperature and 240 °C is equal to 21×10^{-6} K^{-1} which is lower than the CTE measured after complete austenitization, could indicate that the retained austenite is under a compressive stress state [27]. Above 240 °C, the apparent CTE increases up to 41×10^{-6} K^{-1} where the retained austenite transforms into ferrite and cementite.

In the temperature ranges where no transformation occurred, the coefficients of thermal expansion obtained for the ferrite, cementite and austenite are in good agreement with those found in literature (**Table 3,** [20-26]).

A similar evolution of ferrite, cementite and austenite lattice parameters with temperature was observed for heating rates of 10 and 100 °C/s for the different initial microstructures as illustrated for ferrite-pearlite microstructure in **Fig. 4**.

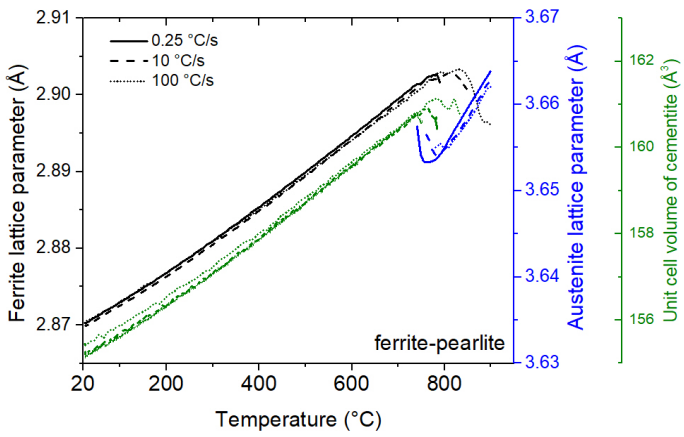

Fig. 4. Ferrite (black) and austenite (blue) lattice parameters and cementite unit cell volume (green) as function of temperature in initial ferrite-pearlite microstructure on heating with different heating rates

The complex variations of mean lattice parameters of each phase can be due to several factors: change in temperature (thermal expansion), elastic strain and change in chemical composition. As the temperature was measured all along the experiment and thermal gradients were negligible, those variations can be further analysed subtracting the thermal contribution using the data reported in **Table 3**.

4.2. Ferrite and cementite lattice parameters before the ferrite + cementite → austenite transformation

First, the mean lattice parameter of ferrite obtained on heating for the three initial microstructures is compared with that of pure iron, heated on the same apparatus and in the same conditions (**Fig. 5**). The absolute values of ferrite lattice parameter for the three initial microstructures are slightly different and are slightly lower as compared to the lattice parameter of ferrite in pure iron. Those differences can be attributed to differences in chemical composition of the ferrite as well as to internal stresses.

The differences in CTE of ferrite in comparison with pure iron are within 3.6% above 450 °C (16.4×10^{-6} K^{-1} in ferrite-pearlite microstructure, 16.2×10^{-6} K^{-1} in the tempered martensite and 16.1×10^{-6} K^{-1} in the bainite, **Fig. 5**).

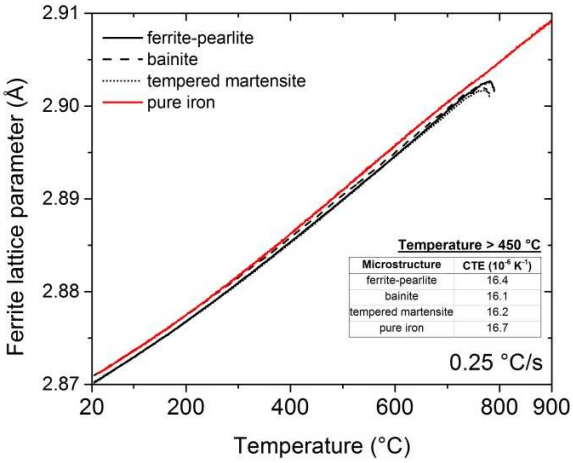

Fig. 5. Comparison of ferrite mean lattice parameter before austenite formation for the three initial microstructures and for the pure iron obtained on heating with a rate of 0.25°C/s. Inset table gives CTE obtained from the experimental curves for the temperatures between 450 °C and A_{C1}

Comparing cementite at room temperature in three initial microstructures and a pure cementite powder [28,29], the mean lattice parameters are quite similar (the differences are within 1%, **Table 4**). Moreover, in the temperature range between 200 and 327 °C, the volume CTE of cementite reported in Ref. [28] is close to 42×10^{-6} K^{-1}, which is in good agreement with the CTE of cementite obtained for the three initial microstructures in the same temperature range: 42×10^{-6} K^{-1} for tempered martensite and lower than 48×10^{-6} K^{-1}

for ferrite-pearlite microstructure. For the temperature range from 450 to 600 °C, the obtained volume CTE of cementite (**Table 3**) is in good agreement with literature data.

Table 4. Mean lattice parameters of cementite at room temperature for different initial microstructures of a 37MnCr4-3 steel in comparison with those for pure cementite powder [28,29]

Microstructure	a (Å)	b (Å)	c (Å)
Ferrite-pearlite	5.0858	6.7374	4.5292
Bainite	5.0860	6.7420	4.5301
Tempered martensite	5.0709	6.7295	4.5484
Cementite powder [28]	5.0809	6.7530	4.5150
Cementite powder [29]	5.0901	6.7456	4.5262

4.3 Mean lattice parameters during the ferrite + cementite → austenite transformation

In order to analyse the lattice parameter evolutions in the transformation temperature range without the thermal contribution, the parameters Δa_{α}, Δa_{γ} and ΔV_{θ} were defined as follows: for each phase, the contribution due to thermal expansion alone was extrapolated from temperature regions where this phenomenon was sole active or predominant, the difference was then calculated between actual measurement and thermal contribution alone. This is schematically illustrated in **Fig. 6**. This was done assuming a constant linear CTE for ferrite and constant volume CTE for cementite given in **Table 3**.

For austenite, the variations of lattice parameter were calculated taking austenite in the single austenite domain as a reference. This is also illustrated in **Fig. 6**, where the extrapolated changes in austenite parameters are shown as a tangent line to the measurements for the high temperature, austenite domain.

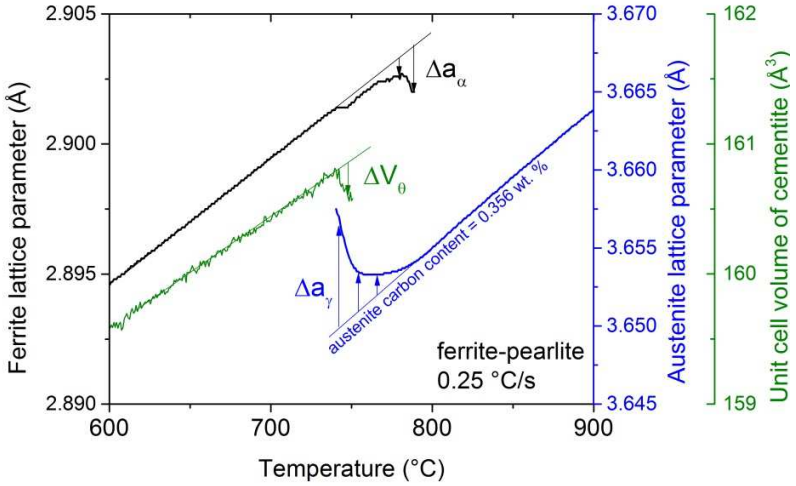

Fig. 6. Ferrite and austenite lattice parameters and cementite unit cell volume obtained for ferrite-pearlite initial microstructure on heating of 0.25°C/s. Δa_{α}, Δa_{γ} and ΔV_{θ} are schematized by arrows.

The resulting variations of Δa_{γ}, Δa_{α} and ΔV_{θ} are plotted versus austenite weight fraction in **Fig. 7a** for ferrite-pearlite microstructure and in **Fig. 7b** for all three initial microstructures (Δa_{γ} and Δa_{α} only).

Δa_{α} slightly decreases at the beginning of the austenite formation and remains nearly constant and equal to -1.5×10^{-4} Å between 20 and 85 wt.% of austenite. A drop to -1×10^{-3} Å is observed between 85 and 100 wt.% of austenite, whatever the initial microstructure.

The Δa_{γ} variations are opposite in sign to those of ferrite, and ten times larger. Δa_{γ} presents the highest value at the beginning of the transformation (0.01 Å) and then decreases as austenite amount increases to reach 0 Å once the transformation is completed whatever the initial microstructure. The decrease is larger at the beginning of the transformation.

ΔV_{θ} decreases continuously with transformation progress. The maximal value is near -0.28 $Å^3$ corresponding to a relative volume change of $5.2\ 10^{-3}$.

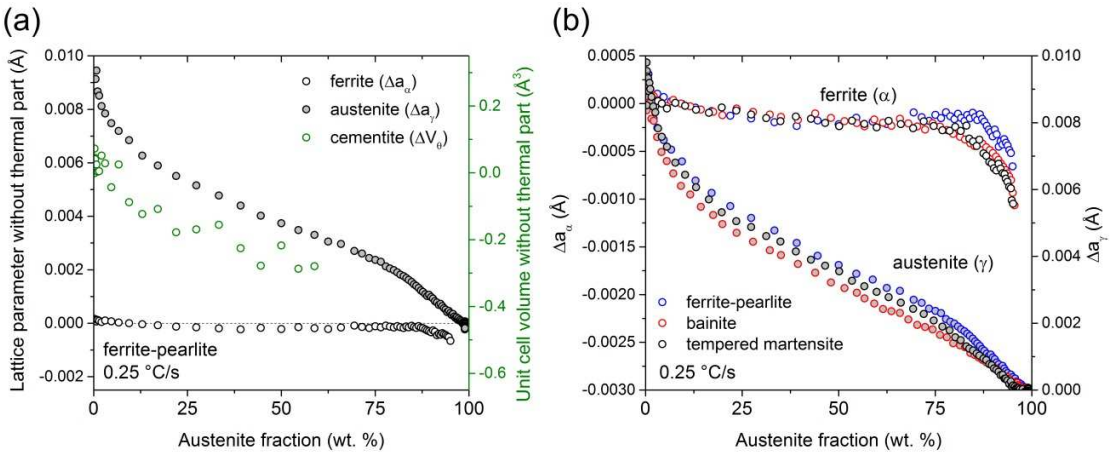

Fig. 7. Variations of mean lattice parameters of ferrite and austenite without thermal contribution (Δa_α and Δa_γ respectively) and unit cell volume of cementite (ΔV_θ) as a function of austenite weight fraction on heating of 0.25 °C/s for (a) ferrite-pearlite and (b) three initial microstructures

The decrease in the mean lattice parameter of ferrite and cementite during the transformation, which is small but significant can be associated with the development of compressive stresses [30] or with a change in its chemical composition.

Since the austenite has a low yield stress in the temperature range where the transformation occurs, the changes in its lattice parameters should be mainly associated with chemical composition variation.

4.4. Austenite chemical composition during austenitization

Considering only the solute elements in the studied steel, we used the relation proposed by Dyson and Holmes [31], as done in Refs. [32-34], for the lattice parameter of the austenite as a function of chemical composition (in wt. %) at room temperature:

$$a_\gamma = 3.5847 + 0.0330 \times [\mathrm{C}] + 0.00095 \times [\mathrm{Mn}] - 0.0002 \times [\mathrm{Ni}] + 0.0006 \times [\mathrm{Cr}] + 0.0015 \times [\mathrm{Cu}] \qquad (1)$$

where 3.5847 Å corresponds to the austenite lattice parameter in the pure iron at room temperature.

Using the composition provided in Table 1, the austenite lattice parameter can be calculated to 3.59789 Å. This is 0.01319 Å greater than for pure iron, with a contribution of 0.01175 Å due to carbon alone, and of 0.00144 Å due to the substitutional elements. Given that the carbon influence is therefore 10 times larger than that of the substitutional elements, the variations of Δa_γ, may be assumed to be mainly related to changes in carbon concentration in austenite ($\Delta w_{c\gamma}$). This is explicited in **Eq. (2)**:

$$\Delta a_\gamma = A \times \Delta w_{c\gamma} \quad (2)$$

with $A = 0.033\ \text{Å}/wt.\%$ [31].

Using **Eq. (2)** and considering that the austenite has the nominal carbon content of the steel, ${w_{c0}}^\gamma$ (**Table 1**), once the austenitization is completed, the mean carbon content in the austenite (${w_c}^\gamma$) can be estimated at any moment of the transformation using the variation of lattice parameter after subtraction of thermal contribution Δa_γ :

$${w_c}^\gamma = \frac{\Delta a_\gamma}{A} + {w_{c0}}^\gamma \quad (3)$$

The result of such estimation is given in **Fig. 8** for ferrite-pearlite and tempered martensite initial microstructures and for different heating rates.

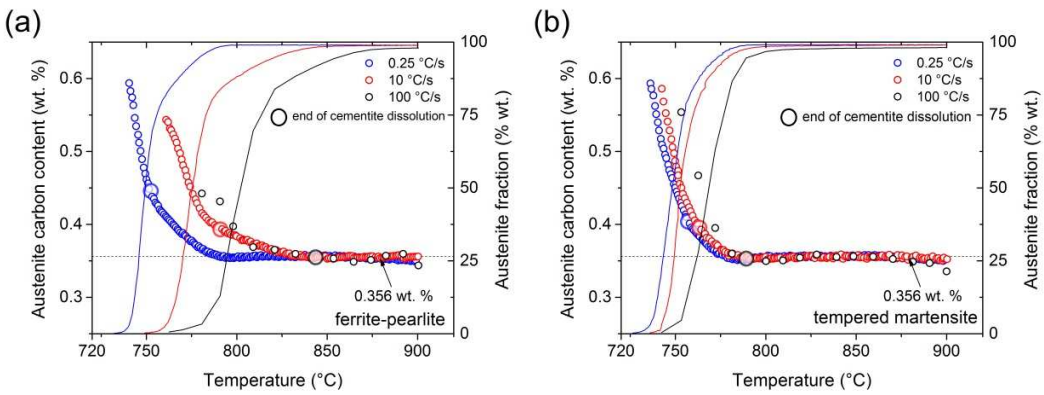

Fig. 8. Mean carbon content in austenite and austenite fraction versus temperature during austenitization for different heating rates and two initial microstructures: a) ferrite-pearlite and b) tempered martensite

Whatever the considered initial microstructure and heating rate, a continuous decrease in the mean carbon content in austenite is observed until the end of the austenitization, when the carbon content stabilizes and remains constant during further heating. The carbon content in the first 3 wt.% of austenite ("initial" austenite mean carbon content) is equal to 0.59 wt.% for the initial ferrite-pearlite microstructure and the lowest heating rate of 0.25 °C/s. An increase in the heating rate leads to an increase in A_{C1} temperature and to a decrease in "initial" mean carbon content in fresh austenite (0.54 wt.% for 10 °C/s and 0.44 wt.% for 100 °C/s). A similar behaviour is observed for the initial microstructure of tempered martensite (**Fig. 8b**) with less difference between the "initial" mean carbon content in austenite for the different heating rates.

Marking the end of cementite dissolution, different stages can be outlined (**Fig. 8**): a first one with a sharp decrease in carbon content in austenite between the beginning of the transformation and the complete dissolution of cementite and a second one with a smoother decrease corresponding to the remaining ferrite dissolution. Once the austenitization is completed, the carbon content in austenite remains constant and equal to the mean carbon content of the studied steel.

When the heating rate increases, the cementite dissolution finishes at higher temperatures and the corresponding mean carbon content in austenite decreases since a higher ferrite amount transforms in austenite before complete cementite dissolution [15].

The mean carbon content evolution in austenite during the two stages of the austenitization in the ferrite-pearlite initial microstructure heated at 0.25 °C/s can be further analysed. From results shown in **Fig. 8**, the carbon content in austenite at the end of pearlite (i.e. cementite) dissolution is about 0.45 wt. % corresponding to the mean carbon content in the

initial pearlite. Indeed, the pearlite fraction estimated by image analysis from images acquired on Scanning Electron Microscope (SEM, **Fig. 1a**) was found to be 80%. Considering that there is no carbon in ferrite, the mean carbon content in pearlite can be roughly estimated as $\frac{0.356}{0.8} = 0.445$ wt.%, which agrees well with 0.45 wt. % estimated from in situ experiment as discussed above.

From **Fig. 8**, we conclude that for the lowest heating rate of 0.25 °C/s, the first formed austenite has a higher carbon content (0.59 wt.%) than the mean carbon content in the initial pearlite (0.44 wt.%). As temperature and austenite fraction increase, the mean carbon content in austenite decreases until reaching the mean carbon content of the initial pearlite at the end of the first stage of the transformation. During the second stage of the transformation, the dissolution of the remaining 20 % of free ferrite with negligible carbon content occurs and the mean carbon content in austenite decreases more smoothly.

In the case of bainitic microstructure, a decrease in mean carbon content in austenite is also observed during the transformation. However, the initial carbon content in austenite increases with the heating rate (**Fig. 9**). Such a result, different from those obtained for the two other initial microstructures should be explained using the microstructural differences in different initial states of the studied steel. Indeed, a small amount of retained austenite was found in the initial bainitic microstructure unlike the ferrite-pearlite and the tempered martensite microstrutures. For the heating rate of 0.25°C/s, the retained austenite completely transforms into ferrite and cementite between 240 and 410 °C. For the heating rates of 10°C/s and 100°C/s, the retained austenite (initial fraction of 3 wt.%) is not completely transformed when reaching A_{C1} temperature and the transformed austenite fraction decreases with increase in heating rate (about 0.7 wt.% at 745 °C for 10 °C/s and 2 wt.% for 100 °C/s). Keeping the assumption that the internal stresses are relaxed in

austenite at those temperatures, the higher carbon content in the austenite when reaching A_{C1} temperature for increased heating rate may be related to the carbon enrichment of the retained austenite during the bainitic transformation [35]. A partial transformation of the retained austenite in ferrite and cementite (heating rate of 10°C/s) could thus lead to a global increase in the carbon content in austenite at the first moment of austenitization (for 3 wt. % of austenite) (**Fig. 9**). Once the A_{C1} temperature is reached and austenite fraction increases, the mean carbon content in austenite starts to decrease due to ferrite+cementite→austenite transformation as for the other microstructures.

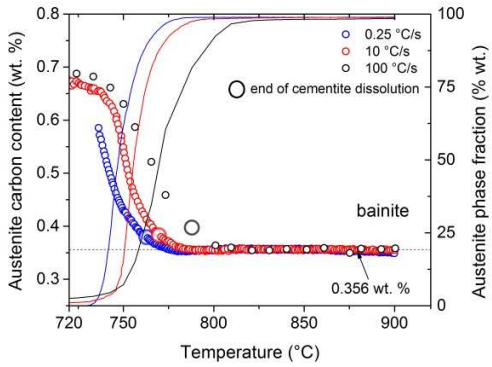

Fig. 9. Mean carbon content in austenite and austenite fraction on heating during austenitization of initial bainitic microstructure for different heating rates

In addition to the mean carbon content in austenite, its chemical homogeneity can be estimated using the FWHM (full-width height middle) of diffraction peaks recorded during in situ experiments. According to Caglioti's equation, FWHM varies with the diffraction angle θ [36]:

$$FWHM = \sqrt{(U \times tan^2(\theta) + V \times \tan(\theta) + W)} \quad (5)$$

where U, V, W are the half-width parameters that can be obtained by Rietveld refinement. First, the diffraction diagrams with the $(111)_\gamma$ and $(200)_\gamma$ peaks are given in **Fig. 10** for three austenite fractions and ferrite-pearlite initial microstructure heated at 0.25°C/s. They illustrate the larger FWHM at the beginning of the transformation (6 wt.% of austenite).

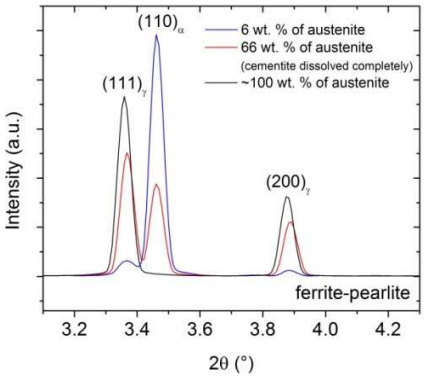

Fig. 10. Austenite diffraction peaks (111) and (200) corresponding to different stages of austenite formation on heating with the heating rate of 0.25 °C/s in initial ferrite-pearlite microstructure: 6 wt.% (beginning), 66 wt.% (end of cementite dissolution) and fully austenitic (end of the austenitization).

The FWHM evolution for $(111)_\gamma$ and $(200)_\gamma$ peaks calculated using the Caglioti's equation (5) are plotted versus temperature in **Fig. 11**[2]. For ease of comparison, the mean carbon content in austenite previously discussed is also reported. A strong continuous decrease in the FWHM of $(111)_\gamma$ and $(200)_\gamma$ peaks is observed during the first stage of the austenite formation followed by a plateau during the second stage (remaining free ferrite dissolution) and later once austenite formation is completed.

An enlargement in diffraction peaks may be due to several factors: small size of diffracting domains, heterogeneities (chemical, internal stresses, local temperature). The decrease in FWHM can be mainly associated with a homogenization of carbon composition of the austenite because stress and thermal gradient during austenite formation as discussed earlier can be considered negligible. Indeed, gradients in carbon content are present during the transformation. The chemical homogenization being controlled by diffusion, is accelerated with temperature. The FWHM of austenite diffraction peaks is thus maximal at the beginning of the transformation due to a maximum chemical heterogeneity. Moreover, it is

[2] As the same evolutions of FWHM for different microstructures with increase in heating rates were observed, Fig. 11 reports the data for three microstructures and three different heating rates.

worth noting that the maximum FWHM increases as the heating rates increase suggesting increase in chemical heterogeneities in austenite.

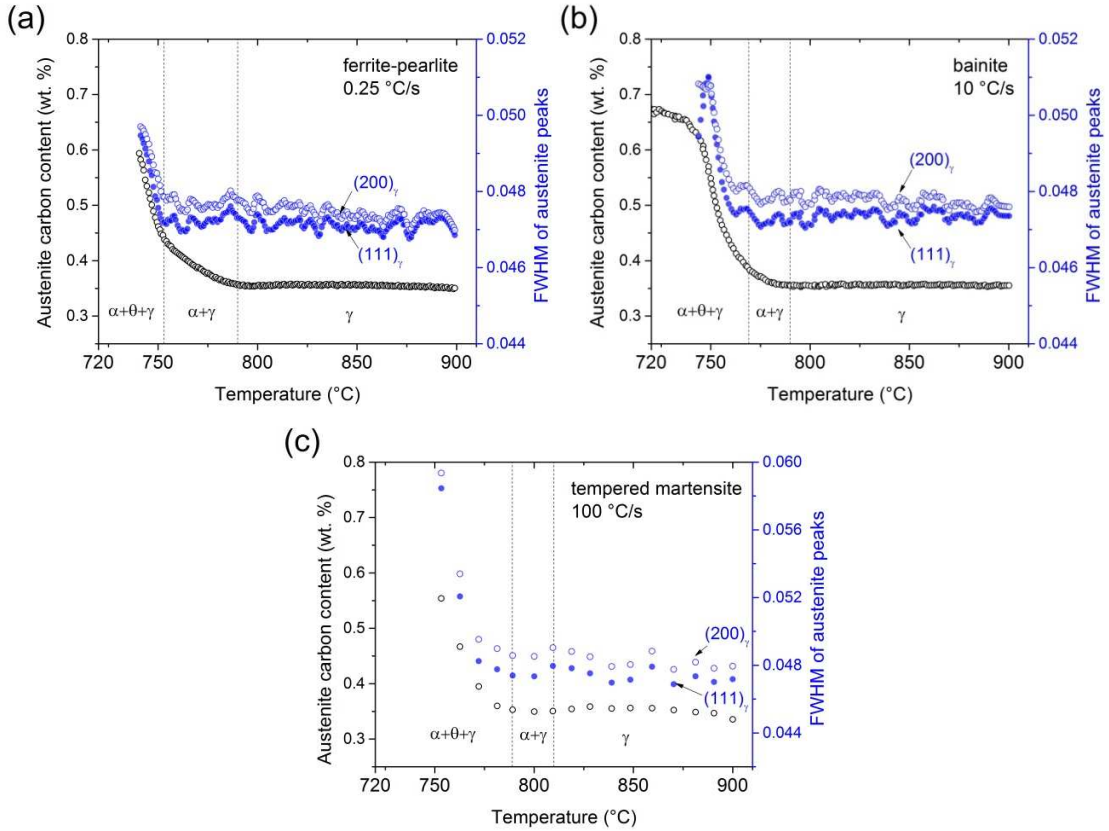

Fig. 11. FWHM of $(111)_\gamma$ and $(200)_\gamma$ diffraction peaks of austenite compared to the mean carbon content evolution during austenite formation for different initial microstructures and heating rates: a) ferrite-pearlite at 0.25°C/s, b) bainite at 10°C/s, c) tempered martensite at 100°C/s

5. Discussion

Since any data for the chemical composition of different phases in different initial microstructures were not available, several assumptions are required for further discussion. Three initial microstructures were obtained at different temperatures and for different durations: 625 °C - 1 h for ferrite-pearlite, 425 °C - 30 min for bainite and 500 °C - 1 h for tempered martensite. These three temperatures and corresponding durations seem to be disadvantageous for a significant diffusion distance of the substitutional elements (Si, Mn,

Ni, Cr, Mo and Cu). Indeed, the estimation of the bulk diffusion lengths in austenite for these elements at the highest temperature of 625 °C for 1 hour annealing, indicate that it does not exceed 10 nm for the fast diffusing elements like Cr and Mn [37]. However, the cementite in pearlite can be significantly enriched in Mn even though the pearlite formation takes place at low temperatures due to accelerated Mn diffusion along the interfaces [38,39]. Nevertheless, diffusion of substitutional elements during the formation of tempered martensite and bainite should be sufficiently limited to be neglected.

Therefore, one can expect the same content of substitutional elements (the same u-fraction) in ferrite in bainite and tempered martensite microstructures while some Mn partitioning could take place during the pearlite formation leading to cementite enriched by Mn. During the austenitization, Mn partitioning can occur as well which depends on initial Mn content in ferrite and cementite [40,41].

We now can analyze the formation of fresh austenite using an isopleth phase diagram obtained for the fixed content of the substitutional elements (according to **Table 1**), except that of Mn, and varying carbon content (at the expense of iron) using Thermo-Calc software and TCFE9 database (**Fig. 12**). In order to take into account possible cementite enrichment by Mn during pearlite formation or during slow heating rate of the three initial microstructures, Mn content in cementite in thermodynamic equilibrium with austenite was being varied when plotting isopleth diagram. However, one can observe that different Mn content in cementite (from 5 to 20 wt. %) in equilibrium with austenite does not change significantly austenite/cementite equilibrium as compared to global content of Mn of 1.285 wt.% (**Fig 12**). Therefore, the discussion can be limited to the nominal Mn content in the studied steel of 1.285 wt.%.

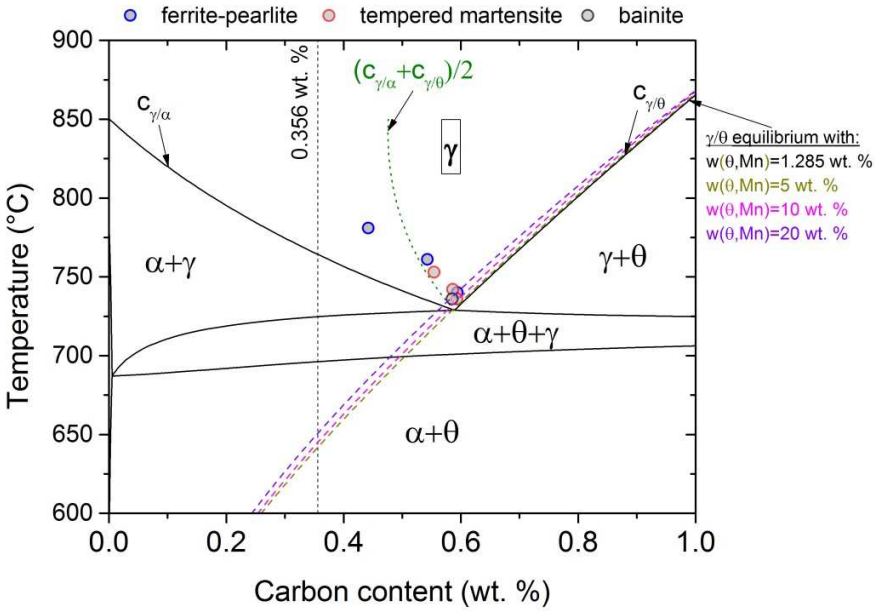

Fig. 12. Isopleth phase diagram for the 37MnCr4-3 steel for fixed content of substitutional elements and varying carbon content (at the expense of iron) obtained using Thermo-Calc software and TCFE9 database. Mn content was taken 1.285 wt.% (black lines) and corresponding to 5, 10 and 20 wt.% (dashed colored lines) of Mn in cementite in equilibrium with austenite to take into account eventual Mn enrichment in cementite during pearlite formation. Initial carbon content in austenite obtained experimentally (points) is compared with the mean carbon content in austenite, which is in thermodynamic equilibrium with ferrite and cementite having the same content of substitutional elements (dotted green line).

The isopleth phase diagram for 1.285 wt. % of Mn (black lines) gives carbon content in the austenite in equilibrium with cementite $c_{\gamma/\theta}$ and ferrite $c_{\gamma/\alpha}$ having the same content of substitutional elements as that in austenite.

Plotting the initial mean carbon content in austenite obtained from the in situ experiments (points in **Fig. 12**), we observe that for the heating rate of 0.25°C/s (the lowest austenite start temperature), the austenite mean carbon content, at the start of austenitization, is close to the eutectoid composition, but nearer to the composition of the austenite at equilibrium with cementite. The carbon content of fresh austenite close to that of eutectoid composition were reported in Refs [4,40,42] and suggested recently in Ref. [15] where austenite formation is starting controlled by carbon diffusion [40,41,43-47].

For different heating rates and ferrite-pearlite and tempered martensite microstructures, a decrease of the mean initial carbon content in austenite is observed when heating rate (and thus the austenitization start temperature (A_{C1})) increases (**Table 5**).

Table 5. Austenite start temperature (A_{C1}) and mean carbon content in austenite at the beginning of austenitization ($C_{0\gamma}$) (3 wt.% of formed austenite) for different heating rates and initial microstructures

Heating rate (°C/s)	Ferrite - pearlite		Tempered martensite		Bainite	
	A_{C1} (°C)	$C_{0\gamma}$ (wt.%)	A_{C1} (°C)	$C_{0\gamma}$ (wt.%)	A_{C1} (°C)	$C_{0\gamma}$ (wt.%)
0.25	740	0.594	736	0.593	736	0.585
10	761	0.543	742	0.586	-	-
100	781	0.442	753	0.554	-	-

When we report all experimental values of initial carbon content in austenite on the isopleth phase diagram, we observe that increasing the heating rate, the initial mean carbon content in austenite varies according to the average value $(c_{\gamma/\alpha} + c_{\gamma/\theta})/2$ (**Fig. 12**). Such a result suggests a linear gradient for carbon content in the first austenite formed between ferrite and cementite [48].

In the case of the ferrite-pearlite initial microstructure and the rate of 100°C/s, a deviation from the average value $(c_{\gamma/\alpha} + c_{\gamma/\theta})/2$ is observed. Eventual partitioning of Mn during austenitization and when forming initial ferrite-pearlite microstructure should be carefully examined for fast heating rate. The assumption of non-linear carbon profile in austenite can be supposed. Experimentally, it requires additional analysis of chemical composition of phases in initial microstructures before austenitization.

6 Conclusion

The influence of heating rate and initial microstructure on the mean lattice parameters of ferrite, cementite and, especially, that of austenite during austenitization was investigated

by in situ HE-XRD in a 0.36C-1.3Mn-0.7Cr-0.07Mo wt.% steel. The main results are summarized below:

(1) Ferrite and cementite are under compression at the end of their transformation into austenite.

(2) During the austenitization, the mean lattice parameter of austenite decreases; this decrease is mainly associated to a change in the mean carbon content.

(3) Assuming that the elastic strains in austenite are negligible, the variations in mean carbon content in austenite are calculated using mean austenite lattice parameter for each transformation condition. The first formed austenite has the highest mean carbon content; it decreases rapidly due to the simultaneous transformation of ferrite and cementite into austenite. Once cementite is dissolved, during the ferrite transformation, the mean carbon content in austenite decreases more slowly.

(4) The initial mean carbon content in austenite at the beginning of the austenite formation is dependent on the heating rate: it decreases as heating rate increases (as clearly shown for ferrite-pearlite and tempered martensite initial microstructures). For the lowest heating rate, the carbon content in the first 3 wt.% formed austenite is near the calculated eutectoid composition obtained by Thermo-Calc and TCFE9 database.

(5) Values of initial carbon content in the first austenite formed are in good agreement with thermodynamic calculations with or without partitioning of Mn in initial cementite.

References

[1] Desalos Y, Le Strat F. Techniques de l'Ingénieur (in French), **M1205** (1996) 1-25

[2] Barglik J, Smalcerz A. The international journal for computation and mathematics in electrical and electronic engineering, Vol. **36** (2017) Issue: 2, 555-564

[3] Kabasakaloglu U, Saruhan H. Materials Testing, Vol. **61** (2019) Issue: 3 277-281

[4] Speich GR, Demarest VA, Miller RL. Metall Trans A **12** (1981) 1419

[5] Roósz A, Gácsi Z, Fuchs EG. Acta Metall **31** (1983) 509-517

[6] Surovtsev AP, Yarovoi VV. Metalloved Term Obrab Met **9** (1984) 2-5

[7] Denis S, Farias D, Simon A. ISIJ Int **32** (1992) 316-325

[8] Caballero FG, Capdevila C, De Andrés CG. ISIJ Int **41** (2001) 1093-1102

[9] Savran VI, Offerman SE, Sietsma J. Metall Mater Trans A **41** (2010) 583-591

[10] Oliveira FLG, Andrade MS, Cota AB. Mater Character **58** (2007) 256-261

[11] Savran VI, Van Leeuwen Y, Hanlon DN, Kwakernaak C, Sloof WG, Sietsma J. Metall Mater Trans A **38** (2007) 946-955

[12] Schmidt E, Wang Y, Sridhar S. Metall Mater Trans A **37** (2006) 1799-1810

[13] Schmidt ED, Damm EB, Sridhar S. Metall Mater Trans A **38** (2007) 244-260

[14] Eggbauer A, Lukas M, Ressel G, Prevedel P, Mendez-Martin F, Keckes J, Stark A, Ebner R. J. of Material Science Vol. **54** (2019) 9197-9212

[15] Esin VA, Denand B, Le Bihan Q, Dehmas M, Teixeira J, Geandier G, Denis S, Sourmail T, Aeby-Gautier E. Acta Materialia **80** (2014) 118-131

[16] Geandier G, Aeby-Gautier E, Settefrati A, Dehmas M, Appolaire B. C. R. Physique, **13** (2012) 257-267

[17] Rietveld H.M. J. Appl. Cryst. **2** (1969) 65-71

[18] Toby Brian H. Powder Diffraction **21** (2006) 67-70

[19] Rodriguez-Carvajal J. Physica B **192** (1993) 55-69

[20] Van Bohemen S.M.C. Scripta Materialia **75** (2014), 22-25

[21] Mohapatra G, Sommer F, Mittemeijer E.J. Thermochimica acta **453** (2007) 31-41

[22] Liu Y. C, Sommer F, Mittemeijer E. J. Phil. magazine **84** (2004) 1853-1876

[23] Kagawa A, Okamoto T, Matsumoto H. Acta metall. **35** (1987) No. 4, 797-803

[24] Hartmann S, Ruppersberg H. Materials Science and Engineering, **A190** (1995) 231-239

[25] Litasov K.D, Rashchenko S.V, Shmakov A.N, Palyanov Y.N, Sokol A.G. Journal of Alloys and Compounds **628** (2015) 102–106

[26] Reed R.C, Root J.H. Scripta Materialia, **38** (1998), No. 1, 95–99

[27] Allain SYP, Gaudez S, Geandier G, Hell J-C, Gouné M, Danoix F, Soler M, Aoued S, Poulon-Quintin A. Materials Science & Engineering **A 710** (2018) 245–250

[28] Wood I. G, Vocadlo L, Knight K.S, Dobson D.P, Marshall W.G, Price G.D, Brodholt J. J. Appl. Crystallogr., **37** (2004), 82–90

[29] Leinewber A. J. Appl. Cryst. **45** (2012) 944-949

[30] Geandier G, Vautrot L, Denand B, Sabine Denis. Materials, 11, **2018**, 1415

[31] Dyson D.J, Holmes B. J. Iron Steel Inst., **208** (1970), 469

[32] Van Dijk N.H, Butt A.M, Zhao L, Sietsma J, Offerman S.E, Wright J.P, van der Zwaag S. Acta Materialia **53** (2005) 5439–5447

[33] Blondé R, Jimenez-Melero E, Zhao L, Wright J.P, Brück E, van der Zwaag S, van Dijk N.H. Materials Science & Engineering A **618** (2014) 280–287

[34] Guo L, Bhadeshia H.K.D.H, Roelofs H, Lembke M.I. Materials Science & Technology, **33**, No. 17 (2017) 2147–2156

[35] Huyghe P, Caruso M, Collet J-L, Dépinoy S, Godet S. Materials Science & Engineering A 743 (2019) 175-184

[36] Caglioti G, Toccheti D. Nuclear instruments and methods, **32** (1965) 181-189

[37] Mehrer. Diffusion in Solid Metals and Alloys. Landolt-Börnstein Handbook (Springer, Berlin, **26** (1990)

[38] Hutchinson CR, Hackenberg RE, Shiflet GJ. Acta Materialia **52** (2004) 3565–3585

[39] Sun WW, Wu YX, Yang SC, Hutchinson CR. Scripta Materialia **146** (2018) 60–63

[40] Enomoto M, Li S, Yang ZN, Zhang C, Yang ZG. Calphad **61** (2018) 116–125

[41] Xia Y, Enomoto M, Yang Z, Lic Z, Zhang C. Philosophical Magazine, **93**, No. 9 (2013) 1095–1109

[42] Jacot A, Rappaz M. Acta mater. Vol. **47** No 5 (1999) 1645-1651

[43] Lai Q, Gouné M, Perlad A, Pardoen T, Jacques P, Bouaziz O, Bréchet Y. Metallurgical and Materials Transactions A Vol. **47**A (2016) 3375-3386

[44] Miyamoto G, Usuki H, Li ZD, Furuhara T. Acta Materialia **58** (2010) 4492–4502

[45] Li ZD, Miyamoto G, Yang ZG, Furuhara T. Mettallurgical and Materials Transactions A **42A** (2011) 1586-1596

[46] Shtansky D, Nakai K, Ohmori Y. Acta Mater **47**, 9 (1999) 2619–2632

[47] Kamoutsi H, Gioti E, Haidemenopoulos GN, Cai Z, Ding H. Metallurgical and Materials Transactions A Vol. **46**A (2015) 4841-4846

[48] Gaude-Fugarolase D, Bhadeshia H. K. D. H., Journal of Materials Science **38** (2003) 1195 – 1201

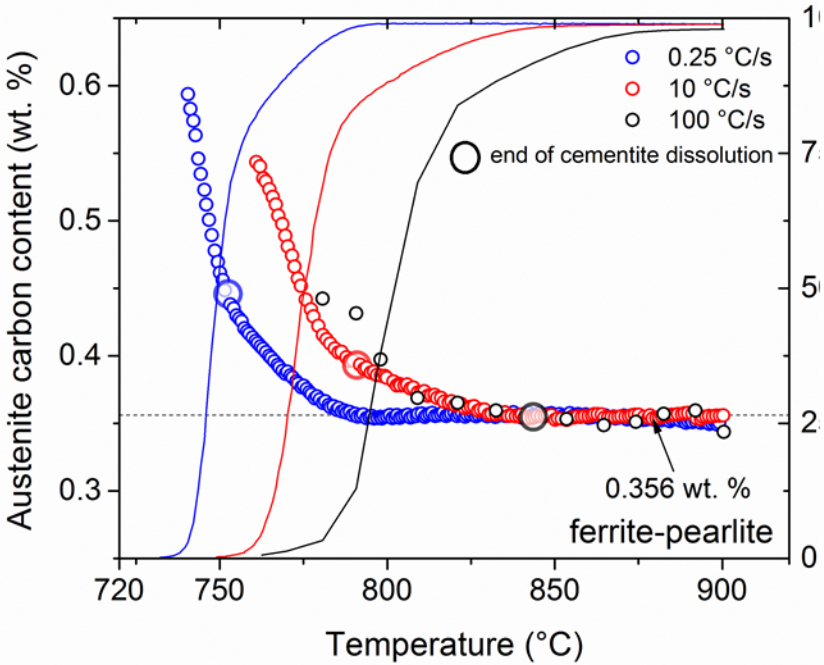
0.25 °C/s
10 °C/s
100 °C/s
end of cementite dissolution
0.356 wt. %
ferrite-pearlite
Austenite carbon content (wt. %)
Temperature (°C)
720
750
800
850
900
0.3
0.4
0.5
0.6
0
25
50
75
100

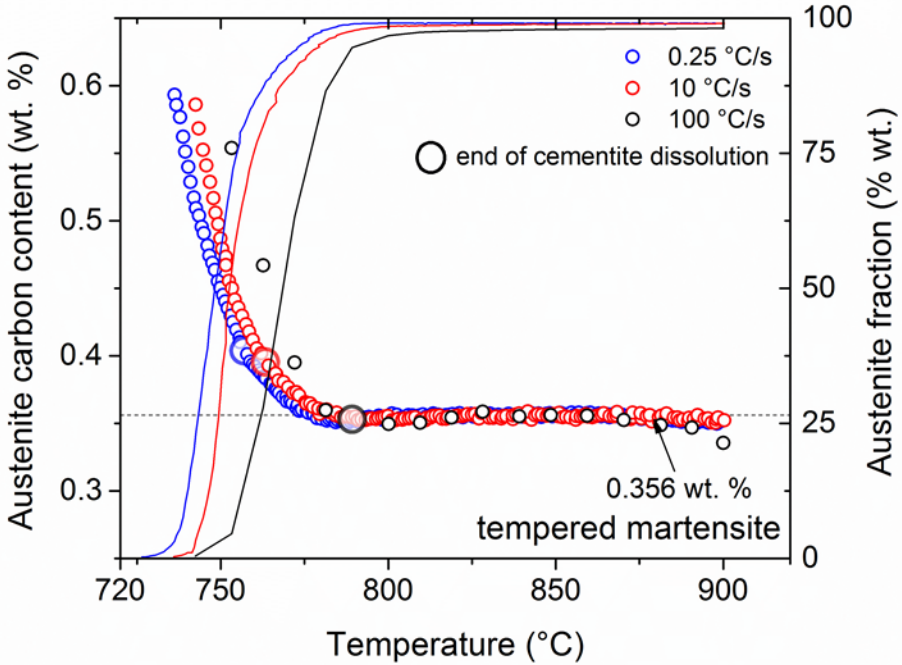
0.25 °C/s
10 °C/s
100 °C/s
end of cementite dissolution
0.356 wt. %
tempered martensite
Austenite carbon content (wt. %)
Austenite fraction (% wt.)
Temperature (°C)
720
750
800
850
900
0.3
0.4
0.5
0.6
0
25
50
75
100